JPn Neuroscience

The Journal of Physiology

J Physiol 590.10 (2012) pp 2453–2469

The role of a trigeminal sensory nucleus in the initiation of locomotion

Edgar Buhl, Alan Roberts and Stephen R. Soffe

School of Biological Sciences, University of Bristol, UK

Key points

- Rhythmic activity is a feature of many regions of the CNS, but surprisingly, no precise pathway for the initiation of locomotion is yet known for any vertebrate.
- Using a well-proven, simple vertebrate system, the hatchling *Xenopus* tadpole, we report here our discovery of a detailed neuron-by-neuron pathway for initiating locomotor activity on one side of the CNS.
- We describe a small population of brainstem neurons (trigeminal interneurons) that are directly excited by trigeminal sensory neurons when the head skin is touched.
- These neurons amplify brief sensory signals and relay excitation to an electrically coupled population of hindbrain reticulospinal neurons (descending interneurons), whose firing initiates swimming locomotion.
- We believe that our discovery of this primitive, direct pathway, which appears simpler than initiation pathways so far defined in invertebrates, is of evolutionary interest and raises the important possibility of equivalent pathways in more complex vertebrates including mammals.

Abstract While we understand how stimuli evoke sudden, ballistic escape responses, like fish fast-starts, a precise pathway from sensory stimulation to the initiation of rhythmic locomotion has not been defined for any vertebrate. We have now asked how head skin stimuli evoke swimming in hatchling frog tadpoles. Whole-cell recordings and dye filling revealed a nucleus of ∼20 trigeminal interneurons (tINs) in the hindbrain, at the level of the auditory nerve, with long, ipsilateral, descending axons. Stimulation of touch-sensitive trigeminal afferents with receptive fields anywhere on the head evoked large, monosynaptic EPSPs (∼5–20 mV) in tINs, at mixed AMPAR/NMDAR synapses. Following stimuli sufficient to elicit swimming, tINs fired up to six spikes, starting 4–8 ms after the stimulus. Paired whole-cell recordings showed that tINs produce small (∼2–6 mV), monosynaptic, glutamatergic EPSPs in the hindbrain reticulospinal neurons (descending interneurons, dINs) that drive swimming. Modelling suggested that summation of EPSPs from 18–24 tINs can make 20–50% of dINs fire. We conclude that: brief activity in a few sensory afferents is amplified by recruitment of many tINs; these relay summating excitation to hindbrain reticulospinal dINs; dIN firing then initiates activity for swimming on the stimulated side. During fictive swimming, tINs are depolarised and receive rhythmic inhibition but do not fire. Our recordings demonstrate a neuron-by-neuron pathway from head skin afferents to the reticulospinal neurons and motoneurons that drive locomotion in a vertebrate. This direct pathway, which has an important amplifier function, implies a simple origin for the complex routes to initiate locomotion in higher vertebrates.

(Received 16 January 2012; accepted after revision 29 February 2012; first published online 5 March 2012)
Corresponding author E. Buhl: School of Biological Sciences, University of Bristol, Woodland Road, Bristol BS8 1UG, UK. Email: e.buhl@bristol.ac.uk

Abbreviations CPG, central pattern generator; dIN, descending interneuron; tIN, trigeminal descending interneuron; vr, ventral root.

DOI: 10.1113/jphysiol.2012.227934

Introduction

Rhythmic activity is a feature of many regions of the CNS and there is a huge experimental and modelling literature about how rhythms are generated. Considerably less attention has been paid to the question of how episodic rhythms are normally turned on by sensory stimuli. While we understand how stimuli evoke sudden, ballistic escape responses (fish Mauthner-cell: Korn & Faber, 2005; crayfish giants: Edwards *et al.* 1999), the precise neuron-by-neuron pathway from sensory stimulation to the initiation of rhythmic locomotion has not been described in any vertebrate. The widely accepted hypothesis, arising particularly from brain stimulation experiments on decerebrate cats in the 1970s (Orlovsky, 1970; reviewed in Orlovsky *et al.* 1999), is that vertebrate locomotion begins, either spontaneously or following sensory stimulation, when descending brainstem reticulospinal pathways become active and turn on spinal central pattern generators (CPGs). These descending brainstem pathways are activated by mesencephalic and diencephalic locomotor regions (Jordan *et al.* 2008). The prevailing view is that the basal ganglia exert tonic inhibition on the locomotor regions and that goal-oriented locomotion can be selected by input from regions such as the cortex or via the thalamus through disinhibition of this suppression by the basal ganglia (Grillner *et al.* 2008). Evidence continues to accumulate suggesting that some of these regions have counterparts in all vertebrates (Stephenson-Jones *et al.* 2011). The organisation and operation of these systems in mammals are highly complex and remain poorly understood. However, precision in defining motor regions, centres and neuronal elements of locomotion-initiating pathways increases significantly as we move to simpler vertebrate species (lamprey: Dubuc *et al.* 2008; zebrafish: Kyriakatos *et al.* 2011).

One way to initiate locomotion in vertebrates is by head stimulation. The decerebrate mammal locomotor system can be activated by electrical stimulation of the trigeminal nerve or its peripheral receptive field (cat: Aoki & Mori, 1981; Noga *et al.* 1988; Beresovskii & Bayev, 1991; rat: Vinay *et al.* 1995). In the lamprey, mechanical stimulation of the head elicits swimming locomotion, and indirect evidence has revealed possible 'relay' neurons placed between trigeminal sensory afferents and the descending, reticulospinal neurons which activate swimming (Viana Di Prisco *et al.* 2005). We study another simple vertebrate with a well-defined motor system, the hatchling frog tadpole, where head skin touch can initiate swimming (Boothby & Roberts, 1995). This paper will define a simple, primitive, sensory pathway from the head skin that excites the descending reticulospinal neurons driving locomotion.

To uncover neuronal pathways initiating rhythmic activity following head skin stimulation, the hatchling *Xenopus* tadpole offers a unique advantage: the excitatory reticulospinal neurons (dINs) which fire on every cycle and drive firing in all other neurons active during swimming have been characterised both anatomically and physiologically (Li *et al.* 2006, 2010; Soffe *et al.* 2009). Initiation of swimming requires the activation of these neurons. Another advantage is that the properties of trigeminal sensory neurons innervating the head skin, and firing briefly to touch, have also been described (Roberts, 1980). Such touch stimuli to the head often evoke swimming where the first flexion is towards the stimulated side (Boothby & Roberts, 1995) and occurs within some 20–30 ms. Here we investigate how brief firing in trigeminal touch afferents leads to the excitation of the reticulospinal dINs that drive spinal cord swim neurons and generate the swimming rhythm. We have characterised the interneurons in a previously unknown trigeminal sensory pathway nucleus. This allows us to propose a pathway by which a head skin stimulus can initiate activity for swimming on the same side as the stimulus. We trace this pathway, step-by-step, from the trigeminal touch-sensitive neurons, through the trigeminal relay nucleus neurons, to the driver reticulospinal interneurons, and finally to the motoneurons which produce the first flexion in swimming.

Methods

Ethical approval

Procedures for obtaining developmental stage 37/38 (Nieuwkoop & Faber, 1956) hatchling *Xenopus laevis* (Daudin) tadpoles comply with UK Home Office regulations. All unregulated experiments on the tadpoles have been approved following local ethical committee review.

Experimental procedures

Tadpoles from a captive breeding colony (13 h:11 h light regime) were briefly anaesthetised in 0.1% MS-222 (3-aminobenzoic acid ester). The dorsal fin was cut open to allow direct access for immobilisation using 10 μM α-bungarotoxin in saline (115 mM NaCl, 3 mM KCl, 2 mM $CaCl_2$, 2.4 mM $NaHCO_3$, 1 mM $MgCl_2$, 10 mM Hepes adjusted to pH 7.4 with NaOH) for 20–30 min. The animals were then pinned to a rotatable Sylgard-coated platform with tungsten wire pins through the notochord. The hindbrain was exposed and its roof removed using a finely etched tungsten pin and fine forceps. Parts of the inner surface of the hindbrain were removed to reveal

neuron somata. The animals were then repinned in a small recording chamber (~1 ml) with saline perfusion, and neuron somata could be seen using a ×40 water immersion lens on an upright Nikon (Tokyo, Japan) E600FN microscope using LED illumination (cf. Safronov *et al.* 2007). Drops of pharmacological antagonists were added to a 100 μl chamber upstream to the recording chamber. The concentrations for 1,2,3,4-tetrahydro -6-nitro-2,3-dioxo-benzo[f]quinoxaline-7-sulfonamide (NBQX) used in this study were 5 μM, 10 μM or 50 μM. NBQX was obtained from Tocris Cookson (Bristol, UK), horseradish peroxidase (HRP) from Boehringer Ingelheim (Bracknell, UK) and all other chemicals from Sigma (Poole, UK). Experiments were performed at 18–22°C.

Electrophysiology

Fictive swimming was initiated by stimulation of the head skin on the right side with either a touch stimulus or with a brief (0.1 ms) current pulse using a fire-polished glass suction electrode with a tip opening of 40–60 μm filled with saline. This excites the peripheral processes of sensory neurons which enter the brain via the trigeminal nerve (Roberts, 1980). To record fictive swimming activity in immobilised tadpoles, similar glass suction electrodes were placed on the right side at the intermyotomal cleft of myotomes 2/3 or 3/4. Extracellular hindbrain and trigeminal unit recordings were made with a similar electrode placed either on the inside of the hindbrain opened at the level of the 2nd to 4th rhombomere or on the trigeminal ganglion. The signals were amplified by a differential amplifier (gain: 1000, SOBS, University of Bristol, UK) and filtered (low: 30 Hz, high: 1 kHz). Whole-cell current clamp recordings were made with an Axoclamp 2B (Axon Instruments Inc., Union City, CA, USA) in bridge mode, filtered (at 30 kHz) and digitised (sampling rate: 10 or 20 kHz, ADC resolution: 16 bit) using a CED Power1401mkII interface (Cambridge Electronic Design Ltd, Cambridge, UK) and Signal 3 and 4 software (CED). Patch pipettes were filled with 0.1% neurobiotin in intracellular solution (100 mM potassium gluconate, 2 mM $MgCl_2$, 10 mM EGTA, 10 mM HEPES, 3 mM Na_2ATP, 0.5 mM NaGTP adjusted to pH 7.3 with KOH) and had resistances of 5–15 MΩ. The liquid junction potential of this solution was measured as +11 mV, but for better comparison with previous data, the values have not been corrected for this.

Anatomy

Neuron anatomy and connections were checked with a standard avidin–biotin technique using diaminobenzidine as chromogen (see Li *et al.* 2001). Briefly, after experiments the animals were left in the saline for 20–25 min allowing the dye to diffuse throughout the whole cell. The animals were fixed in 2% glutaraldehyde for at least 2 h, washed in phosphate-buffered saline (PBS, 120 mM NaCl in 0.1 M phosphate buffer) and again in PBS containing 1% Triton X-100 before labelling with ExtrAvidin (1:200) for 3 h. The animals were then washed again in 0.1 M PBS, the neurons stained in 0.8% DAB in phosphate buffer, and then washed again in buffer containing 0.03% H_2O_2 for 5 min each. After washing in tap water, the brain and spinal cord were exposed and the specimen dehydrated in an ascending alcohol series and cleared in methyl benzoate. Specimens were mounted ventral side down between coverslips with DePeX on a reversible aluminium microscope slide. Once mounted, the hindbrain lay opened along the dorsal midline like a book. Neurons were observed using a ×100 oil immersion lens and traced using a drawing tube. Photographs of the brain were obtained using a ×20 objective lens and a CCD camera (DeltaPix DP 200, Maalov, Denmark) and arranged in Adobe Photoshop (Adobe Systems Inc., San Jose, CA, USA). Measurements were made from the scale drawings and corrected for shrinkage during processing (×1.28). The position of the recorded cell bodies was measured during recording using a micrometer connected to the microscope. It is possible that cell bodies could move and change shape slightly during recording and processing.

Spinal cord backfills

To identify and measure the whole population of tINs, their somata were labelled retrogradely from their axons in the spinal cord. For this the animals were immobilised, mounted on a rotatable Sylgard platform and the spinal cord exposed. The left half of the spinal cord was severed just caudal to the hindbrain to avoid contralateral labelling. A vaseline well was built around the spinal cord approximately at the middle of the animal, filled with intracellular solution containing 0.1% neurobiotin and the spinal cord cut to allow the dye to enter the axons. The neurobiotin solution was removed after 30–45 min and the animal fixed and processed as above. In a few additional examples, HRP was made up in concentrated aqueous solution and dried onto the tip of an etched tungsten needle. One side of the spinal cord was then crushed between a clean needle placed on the midline and an HRP-coated needle placed on the lateral surface of the cord. After 2 min the embryo was transferred to 75% physiological saline that was further diluted as the wounds healed, fixed after 4–6 h and processed as above. Transverse sections of the hindbrain were obtained by embedding the processed animals in wax and cutting 10 μm-thick slices on a microtome.

Modelling

To study the summation of tIN EPSPs in dINs we used a simple model of a synapse generated in Minitab v.13 (Minitab Inc., State College, PA, USA). After selecting a particular tIN population size, the timing of all spikes fired by that population was set relative to time $t = 0$ (equivalent to the time of a single skin stimulus). The total number of spikes depended on the size of the tIN population and the proportion firing one to five spikes (1.00, 0.48, 0.24, 0.09 and 0.03, respectively). The timing of each spike was set randomly from physiological data within ranges measured separately for each spike order (first to fifth; 3.9–36.7 ms overall). Using a probability of 0.5 based on the observed synaptic failures, each spike could then generate a unitary EPSP, modelled conventionally as the sum of two exponentials:

$$V(t) = 1/(\tau_1 - \tau_2) \times (e^{(-t/\tau_1)} - e^{(-t/\tau_2)})$$

where time constants τ_1 and τ_2 were selected to produce an EPSP that matched measured mean time to peak (4.0 ms) and duration at half-amplitude (13.9 ms). The peak amplitude of each unitary EPSP was scaled randomly within the distribution of measured amplitudes (2.26 ± 1.01 mV). All the individual EPSPs were then summed linearly according to their presynaptic tIN spike times. To take into account the synaptic driving force, the resulting compound EPSP trajectory was finally corrected by re-simulating it in 0.1 ms steps as:

$$V'_{(t)} = V'_{(t-1)} + [(51 - V'_{(t-1)})/51][V_{(t)} - V_{(t-1)}]$$

where V' is the corrected voltage and the constant (51) is the synaptic driving force at rest, given by the difference between the mean dIN resting potential and the EPSP reversal potential (assumed to be 0 mV).

Data analysis

Data analysis was performed using routines purpose-written for Minitab. The latencies of post-synaptic potentials (EPSPs and IPSPs) or the first action potential were measured as the time between the peak of the presynaptic action potential or stimulus and the onset of the PSP (or the peak of the postsynaptic action potential) and averaged for each cell/connection type. Additionally for EPSPs the 10–90% rise time, the time to peak and the width at half-peak-amplitude were measured. In patch-pipette recordings from pairs of neurons, current-induced spikes in one cell caused a small cross-talk artefact in the other (see Li *et al.* 2002). These artefacts were removed from some recordings in which they obscured the onset of small EPSPs evoked by current-induced spikes. To do this, either averaged records of EPSP failures (artefact alone) or smoothed, differentiated spike traces were subtracted from EPSP records (EPSP plus artefact). The recorded traces, photographs and drawings were imported into and the figures finally arranged using Corel Draw (Corel Corp., Ottawa, ON, Canada). Statistical tests used are stated in the Results. The outcome of tests was regarded as significant where $P < 0.05$. All measurements are expressed as mean ± standard deviation (SD).

Results

Trigeminal sensory interneurons responding to head stimulation

Briefly touching or stroking the head of the tadpole initiates the swimming rhythm (at 10–25 Hz; Roberts, 1990) and will excite trigeminal mechanosensory neurons innervating the head skin (Roberts, 1980). Counts of axon numbers in the ophthalmic and maxilliary trigeminal nerves and measures of the receptive field areas of individual sensory neurons suggest that there are 50–80 touch-sensitive trigeminal afferents on each side of the head (Hayes & Roberts, 1983). The axons of these neurons project from the trigeminal ganglia to descend as a compact tract, some 20 μm in dorso-ventral extent, through the ipsilateral hindbrain. Some axons reach as far as the rostral spinal cord. To search for groups of sensory interneurons which might be contacted by these descending trigeminal axons, we used neurobiotin to retrogradely label hindbrain neurons projecting into the right side of the spinal cord in eight tadpoles. We also examined earlier material retrogradely labelled with HRP. Many ipsi- and contralateral neurons were seen, including a consistent ipsilateral group of 14–23 neurons in a mid-dorsoventral position lying in the region of cranial nerve VIII in rhombomeres 2–4 (Fig. 1*A*).

Extracellular recordings were therefore made from the right side of the hindbrain caudal to the trigeminal nerve entry in rhombomeres 2–4 in three tadpoles to search for activity during natural sensory stimulation of the head skin. Strokes with a fine hair (10 μm diameter) evoked unit firing (Fig. 1*Ba*). These units fired to strokes anywhere on the same side of the head and, unlike the primary afferent neurons (Roberts, 1980), did not have local receptive fields. In some cases activity in these units was followed by swimming. They did not fire to strokes elsewhere on the body or tail (Fig. 1*Bb*), which were also sometimes sufficient to initiate swimming.

When making whole-cell recordings from brain neurons, electrical stimulation of the skin has to be used as adjacent mechanical stimulation dislodges the electrodes. We therefore made extracellular recordings from trigeminal neurons in the ophthalmic ganglion of six tadpoles to test what response they gave to a 0.1 ms current pulse given to the head skin with a small electrode placed rostral and dorsal to the eye. As the stimulus increased

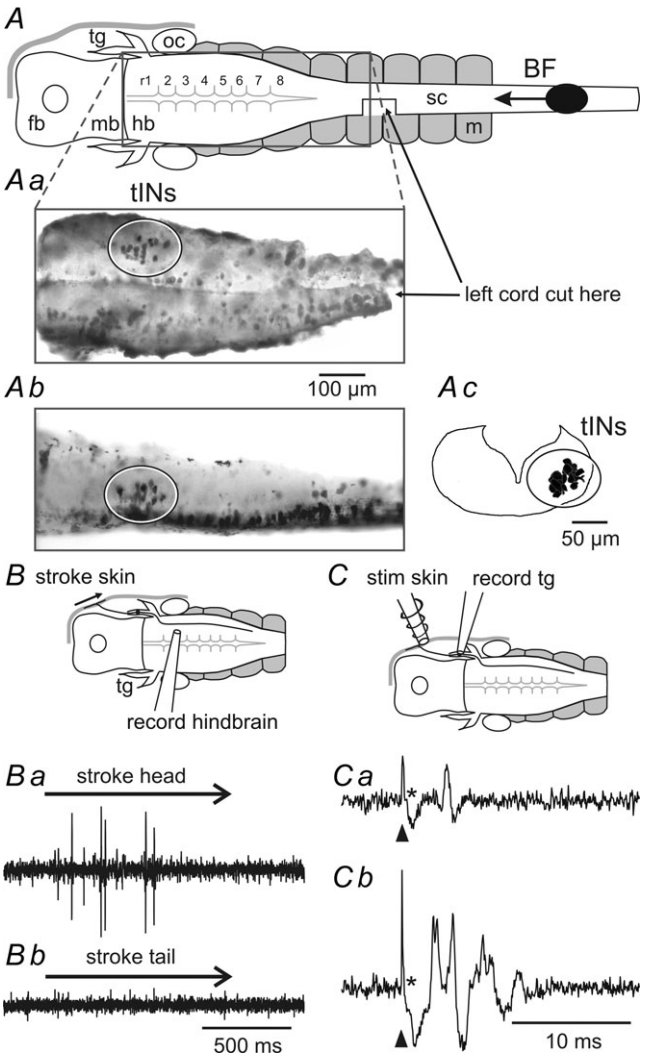

Figure 1. Retrograde filling and extracellular recordings of possible trigeminal interneurons in the hindbrain and trigeminal afferents
A, diagram of the CNS in dorsal view to show the main regions, place where left spinal cord was cut and site of neurobiotin application (BF). *Aa*, inset (photograph) shows a cluster of neuron somata in the hindbrain (tIN, ellipse) revealed by backfilling their axons from the ipsilateral spinal cord (rostral left). *Ab*, photograph of the same region in a different animal in lateral view (rostral left, dorsal up). *Ac*, composite drawing of 11 transverse sections of the hindbrain around the otic capsule (dorsal up) showing the labelled neurons on the right side (ellipse). BF, direction of backfill; fb, forebrain; hb, hindbrain; mb, midbrain; m, muscles; oc, otic capsule; sc, spinal cord; tg, trigeminal ganglion, r1–8, rhombomeres. *B*, diagram of set-up to stimulate head skin and record from hindbrain neurons. *Ba*, record shows firing to head skin stimulation (stroke with hair at arrow). *Bb*, unit in *Ba* shows no firing to tail skin stimulation. *C*, diagram for head skin stimulation and trigeminal neuron recording. *Ca*, trigeminal ganglion recordings show a single unit at threshold in response to a short electrical stimulus (arrowhead). *Cb*, a stronger stimulus evokes firing in more units. Asterisks mark the stimulus artefacts.

to around the threshold to elicit swimming, a clear single unit appeared at 3.4 ± 0.5 ms (SDs for individual units ranged from 0.1 to 0.3, mean 0.2); with further increase, firing occurred earlier and other units appeared (between 2.9 ± 0.6 ms and 6.5 ± 1.5 ms); no units fired later than 9.3 ms or multiply (Fig. 1*C*). These recordings therefore suggest that a 0.1 ms current pulse to the head skin, of sufficient intensity to elicit swimming, excites the free nerve endings of a small number of sensory neurons, each of which only fires a single action potential.

Characterisation of trigeminal sensory pathway interneurons (tINs)

Since extracellular recordings had shown activity in the hindbrain caudal to the trigeminal nerve in response to head skin stimulation, we used whole-cell recordings to locate neurons in this region firing in response to a 0.1 ms current pulse to the skin on the same side of the head. Such neurons might form the first link in a pathway for the initiation of swimming (Fig. 2). We made whole-cell recordings from 37 neurons with somata in the 2nd to 4th rhombomeres. These neurons were silent at rest but were excited to fire by head skin stimulation. We will first define the anatomy revealed by neurobiotin-filling of this previously unknown type of trigeminal descending interneuron (tIN), excited by head skin stimulation.

The 37 recorded and neurobiotin-filled tINs showed a consistent set of morphological characteristics: (a) somata (diameter: 10–20 μm) are mainly unipolar and form a group in the hindbrain (range: 150–330 μm from mid-hindbrain border and 30–150 μm from midline; Fig. 3*A*, see also Fig. 1*A*); (b) dendrites range from simple (Fig. 2*B*) or compact (Fig. 2*F* and *H*) to relatively extensive (Fig. 2*E*, *D* and *G*) and extend into the region where they could receive *en passant* synaptic contacts from the descending axons of trigeminal sensory neurons (Hayes & Roberts, 1983); (c) a long ipsilateral descending axon projects either directly from the soma or from primary processes and initially is directed medio-ventrally before descending into the spinal cord (length: 1.75 ± 0.48 mm; Fig. 3*B*). Many axon lengths may be underestimates as staining faded and there was no distinct end-bulb ($N = 24$) or axons could not be traced to the end because the spinal cord was damaged during processing ($N = 10$). The lengths of the three axons with a clear end-bulb and thus filled to the end were 2.0, 2.0 and 2.7 mm. The axons had uneven diameters, were relatively thick for the tadpole (up to $\sim$1 μm), and sometimes had short side branches (Fig. 2*B*, *F* and *G*).

In all whole cell experiments examining responses of tINs to head skin stimulation, we also recorded ventral root activity so that we could determine the threshold stimulus current required to initiate swimming

(threshold = 100%). All recorded tINs, after stimulation of the head skin at swimming threshold, received a large, short latency EPSP followed by a spike. The effect of stimulus intensity was analysed in 21 of these. The intensity to evoke an EPSP without a spike was 86 ± 8% of the swim threshold, and when the stimulus was at 94 ± 6%, all tINs fired a spike. Spiking in individual tINs could thus occur without subsequent swimming (18/21); however, in only 4/21 tIN recordings did swimming occasionally start without a spike in the recorded tIN. Spikes in tINs reached their peak 5.4 ± 1.6 ms (N = 34 tINs) after the stimulus. Increasing the stimulus strength made tIN spiking more reliable; the first spike could become earlier (by up to 2 ms) and multiple firing often occurred (starting from 5 ± 7% above swim threshold). With further increase of the stimulus, the burst became longer (up to 6 spikes, instantaneous frequency >250 Hz), but 10/34 tINs only ever fired once. The excitatory responses of tINs could also be followed by IPSPs (arrows, Fig. 2).

The large EPSPs produced in tINs by trigeminal afferents were analysed when weaker head skin stimuli did not evoke a spike (Fig. 4*B*). For each of 23 tINs, 5–15 EPSPs were measured: latencies were 4.4 ± 0.5 ms, amplitudes 14.2 ± 5.4 mV, rise times from 10 to 90% amplitude 2.5 ± 1.0 ms, time to peak 8.7 ± 1.8 ms after the stimulus, and duration at 50% amplitude 17.8 ± 10.8 ms. In 13 tINs where the stimulus current was held constant, the standard deviations of latencies of five EPSPs in each tIN ranged from 0.1 to 0.3 ms (mean 0.2). The tIN EPSP latencies are therefore only 1 ms longer than the latencies of afferent spikes recorded from the trigeminal ganglion (see above) and have equally small standard deviations. We

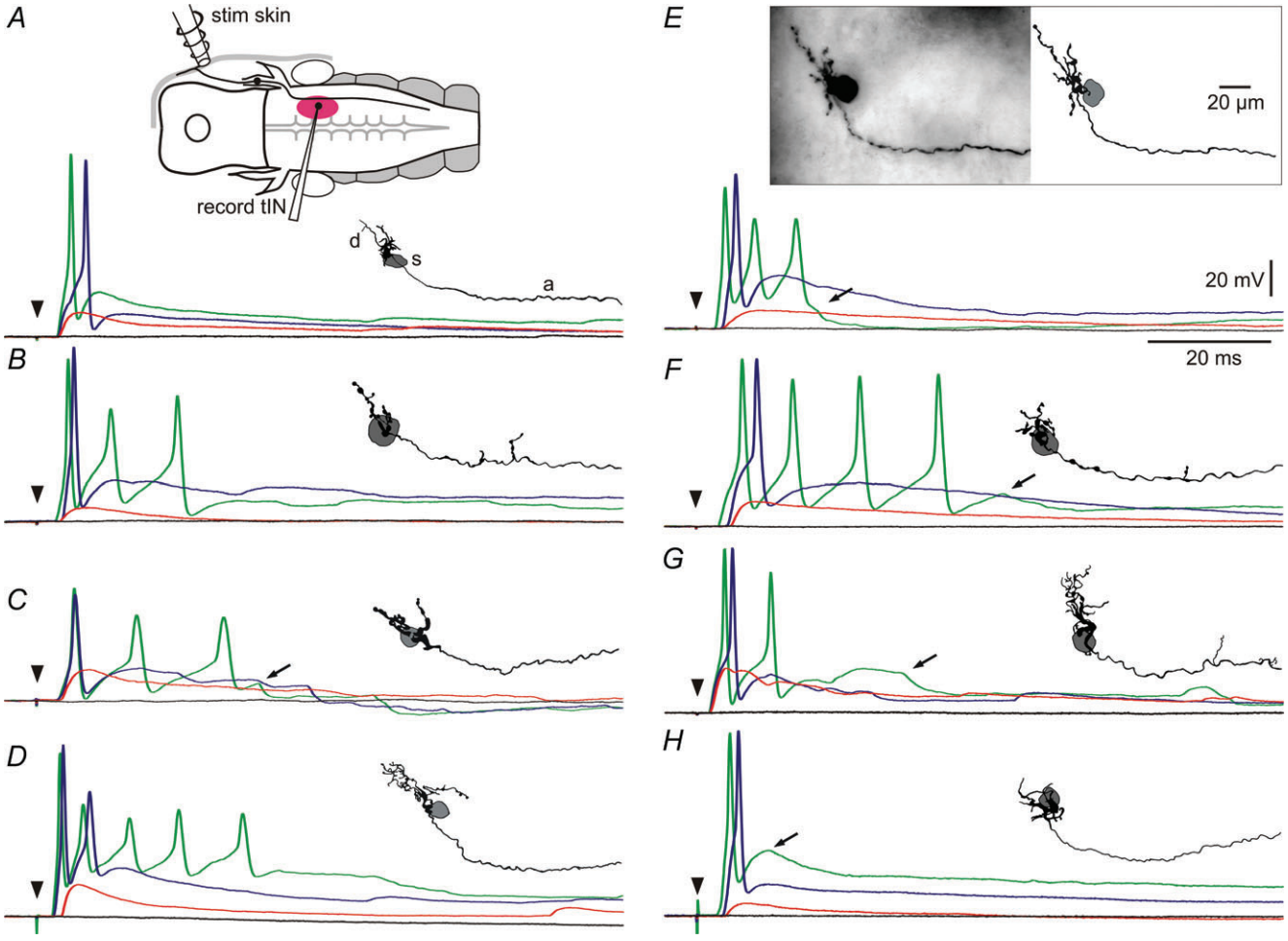

Figure 2. Anatomy of trigeminal interneurons (tINs) and responses to head skin stimulation
A, diagram of the preparation viewed dorsally showing the head skin stimulating electrode (stim skin) on the right side, a trigeminal sensory neuron projecting into the brain and the area where tINs were recorded (purple ellipse; record tIN). Traces show tIN responses to skin stimuli (arrowhead) of increasing strength from black = no response, red = EPSP alone, blue = spike, to green = multiple or earlier spikes. Inset shows the morphology of the tIN viewed from the inside of the right side of the hindbrain (rostral left) with dendrites (d) and descending axon (a). The position of the soma (s) is shown in grey. *B–H*, further examples to show the range of tIN anatomy and responses; *E* includes a photograph of the filled tIN. Arrows in *C*, *E*, *F*, *G* and *H* mark IPSPs (see text).

conclude that tINs are directly, monosynaptically excited at synapses from trigeminal sensory axons.

To investigate the receptors activated during tIN EPSPs we bath applied the glutamate AMPA receptor (AMPAR) antagonist NBQX (5–50 μM). A rapidly rising, large first component was blocked by NBQX ($N = 18$; Fig. 4*D*) and is therefore AMPAR mediated. A second, smaller component was only visible in NBQX, had the same latency (4.1 ± 0.6 ms; Mann–Whitney test: $U = 129$, $n_{1,2} = 23,15$, $P = 0.1983$), but was smaller (peak amplitude: 4.7 ± 1.7 mV; $U = 5$, $n_{1,2} = 23,15$, $P < 0.0001$), slower rising (time to peak 16.6 ± 7.3 ms; 10–90% amplitude in 10.4 ± 6.4 ms; $U = 21$, $n_{1,2} = 23,15$, $P < 0.0001$) and longer lasting (width at 50% amplitude: 54.4 ± 27.5 ms; $U = 26$, $n_{1,2} = 23,15$, $P < 0.0001$; $N = 15$ tINs) and was therefore probably NMDAR mediated.

On the basis of our extracellular recordings, we suspected that individual trigeminal afferents would contact multiple tINs and conversely that individual tINs would receive excitatory synapses from many head skin afferents. To get direct evidence for the first of these, we made simultaneous recordings from six pairs of tINs. When a skin stimulus just reached the level to evoke an EPSP in one tIN (presumed to be the threshold level to activate a single trigeminal afferent; see Fig. 1*Ca*), an EPSP always appeared in the second tIN of the pair. Since different tINs had slight differences in spike threshold, the same weak stimulus could elicit a spike in only one despite eliciting an EPSP in both. As well as showing that single afferents do apparently excite multiple tINs, these paired recordings also showed that tINs do not excite or inhibit each other and show no evidence of electrical coupling.

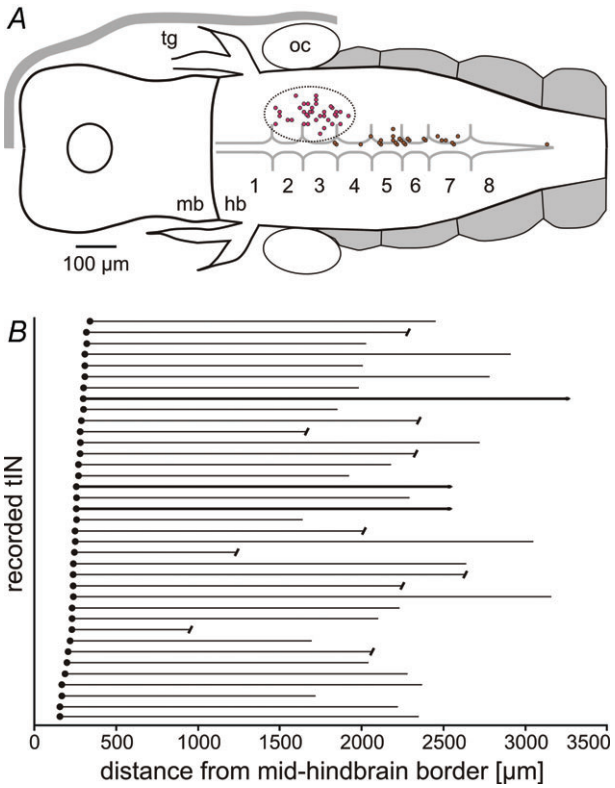

Figure 3. tIN soma positions and axon lengths
A, positions of the somata of recorded tINs (in dotted outline in rhombomeres 2–4) and dINs (close to midline in rhombomeres 3–7). *B*, individual tIN soma positions (filled circles) and descending axons. Some axons were broken (capped lines) or faded out but 3 were completely filled (bold lines).

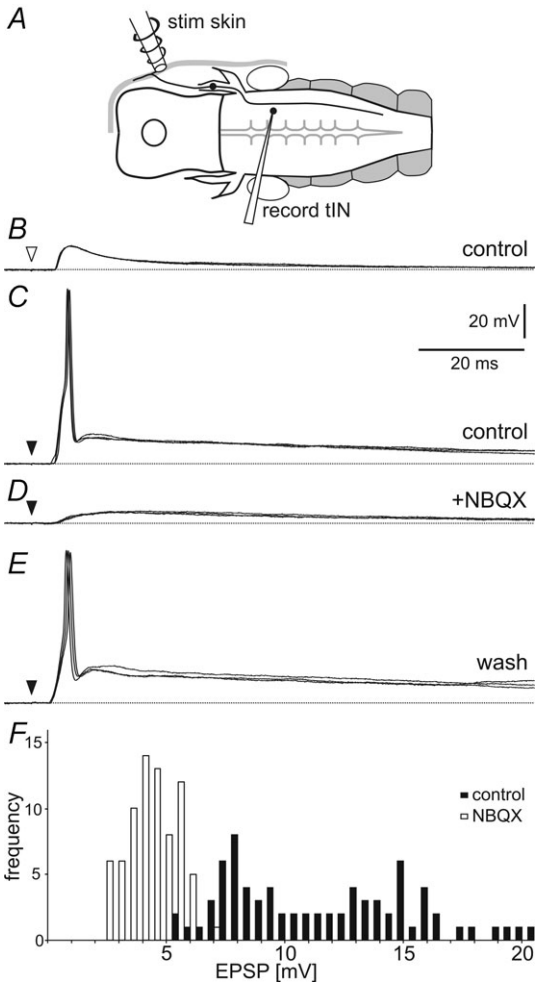

Figure 4. Effects of NBQX on EPSPs in tINs evoked by head skin stimulation
A, diagram of the preparation in dorsal view showing the position of the stimulating and recording electrodes. *B*, a current pulse to the head skin (open arrowhead) leads to a tIN EPSP with a short delay. *C*, a stronger stimulus (black arrowhead) leads to spiking. *D*, NBQX perfusion (50 μM) blocks the spike and reveals a smaller slow rise and fall EPSP. *E*, after 20 min washing, the same stimulus evokes spiking again. Overlay of three traces each, dotted lines show resting membrane potential. *F*, histogram showing the tIN EPSP amplitude before (black bars) and after NBQX perfusion (open bars). Data are from 5 EPSPs from 15 tINs for each treatment, bin size: 0.5 mV.

Lastly, excitation of multiple tINs by each sensory afferent was indicated by the observation that we could always find several tINs responding to stimuli at a single site in individual animals.

We next investigated the range of afferent input to individual tINs. Trigeminal sensory afferents have rather localised receptive fields in the head skin (area: $\sim$0.015 mm^2, diameter: $\sim$200 μm, Roberts, 1980). To test whether tINs also have local receptive areas, one stimulating electrode was placed on the skin rostral and dorsal to the eye in the area innervated by the ophthalmic branch of the trigeminal nerve, and another was placed caudal and ventral to the eye in the area innervated by the maxillary branch, at a spacing of $>$500 μm. EPSPs and spikes were evoked by just supra-threshold stimuli at either location in four recorded tINs showing that they do not have local receptive fields but receive input from widespread head skin afferents. In contrast, tINs did not spike in response to current pulse stimuli given to the trunk or tail skin on the same side ($N = 18$), or to stimuli at any location on the other side of the animal ($N = 19$). They were also not activated when stronger stimuli at the same locations evoked a skin impulse which propagates from cell to cell through the skin and can start swimming ($N = 7$; Roberts, 1969). Finally, tINs did not fire as a result of dimming the illumination which excites the pineal eye and can also start swimming ($N = 35$; Foster & Roberts, 1982). We therefore conclude: that tINs respond only to head skin stimulation on the same side; that individual trigeminal afferents contact multiple tINs; and that individual tINs receive synapses from widespread trigeminal afferents.

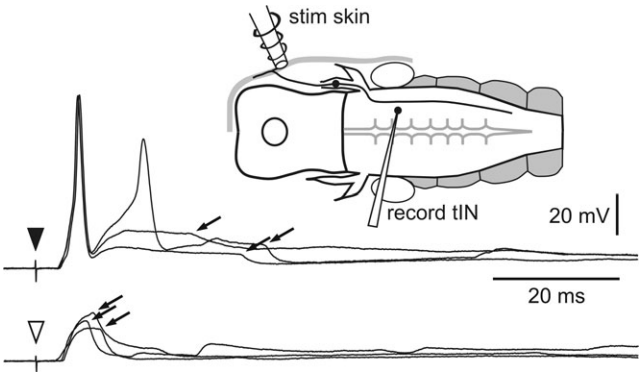

Figure 5. Inhibition of tINs after head skin stimulation
A tIN receives IPSPs (arrows) following head skin stimulation (arrowhead). IPSPs also occur following a weaker stimulus (open arrowhead), insufficient to evoke a spike. These IPSPs occur earlier and are not masked by a spike.

As well as being excited by head skin stimulation, tINs can also receive early inhibition. IPSPs were seen with or without firing in an individual tIN (Figs 2 and 5) and with or without subsequent swimming activity, but never without previous EPSPs. Inhibition may be obscured by tIN firing, but clearly occurred at short latency following a stimulus in cases where the tIN did not fire (mean latency of earliest IPSPs: 9.7 $\pm$ 3.0 ms, minimum: 4.5 ms;

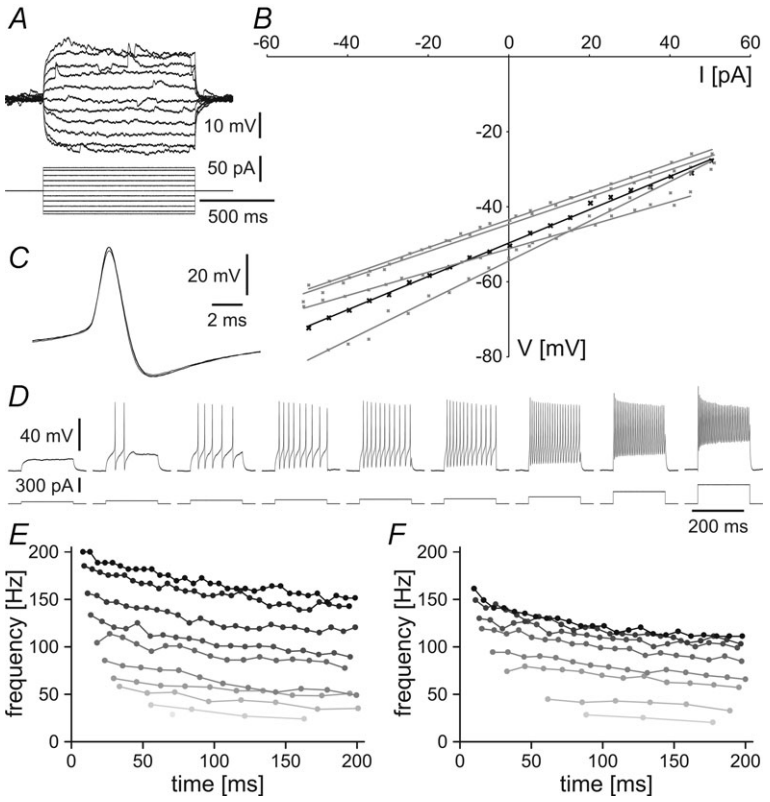

Figure 6. Neuronal properties of tINs
A, response to injected current: Membrane potential change of a typical tIN (R_{in} of 372 MΩ) in response to applied depolarising and hyperpolarising current. *B*, input resistance: plot showing the current–voltage relationship for the cell shown in *A* (black trace) and four other tINs (R_{in} from 312 to 529 MΩ) around the resting membrane potential. *C*, spike shape: tINs have narrow spikes with clear afterhyperpolarisation as shown in an overlay of three traces of a tIN spike evoked during current injection. *D*, firing response: a tIN shows non-adapting, repetitive firing (up to 200 Hz) to depolarising current injections with increasing intensity. *E* and *F*, plots showing that the instantaneous firing frequency of two tINs increases as a function of the injected current (from 40 to 300 pA, grey to black), staying relatively constant within a burst. *E* is same neuron as *D*.

$N = 27$ tINs). These short latency IPSPs suggest there may be some direct connections from trigeminal afferents onto currently unknown inhibitory trigeminal interneurons. Such inhibition could limit the occurrence or duration of tIN firing following a head skin stimulus.

Cellular parameters were measured for 27 tINs. Resting membrane potentials were -55 ± 6 mV and input resistances 459 ± 173 MΩ (measured from the *I–V* regression lines fitted to voltage responses to injected positive and negative current steps around the resting potential; Fig. 6*A* and *B*). Measured relative to 0 mV, action potential peak was 22 ± 5 mV, firing threshold estimated from the inflexion in the upstroke of the spike was -16 ± 4 mV, and spike width at half-amplitude was 1.2 ± 0.3 mV. Spikes had a pronounced after-hyperpolarisation (trough: -39 ± 6 mV at 2.5 ± 0.5 ms after spike peak; Fig. 6*C*). When depolarising current (200 ms) was injected just above the threshold to elicit firing, tINs fired one or a few spikes. When the current was increased, all tINs fired repetitively and spiking frequency increased up to around 100–200 Hz ($N = 27$ tINs; Fig. 6*D–F*). During current-induced repetitive firing, instantaneous frequency dropped only slightly, spike amplitude decreased and spike width increased.

During swimming, most (29/36) tINs were depolarised by up to 10 mV (Fig. 7) and this depolarisation could persist for up to 500 ms after the end of a swimming episode (see also Fig. 12*G*). However, tINs did not receive any obvious rhythmic excitation during swimming and they did not fire (emphasising their characteristic of firing only immediately after a head skin stimulus). Instead, most tINs were rhythmically inhibited and IPSPs tended to decrease in amplitude as swimming continued. Of the 36 tINs examined, 12 received predominantly on-cycle inhibition (in phase with ventral root discharge on the same side; Fig. 7*A*) and 19 received predominantly mid-cycle inhibition (Fig. 7*B*), though occasional IPSPs showed no obvious coupling to the swimming rhythm. The remaining five tINs received no rhythmic inhibition.

In summary, our evidence shows that tINs form a localised group, or nucleus, of around 20 hindbrain interneurons at the level of the VIIIth nerve, with long axons projecting ipsilaterally to the spinal cord. They are strongly and monosynaptically excited via glutamatergic (mainly AMPAR mediated) synapses from the descending axons of trigeminal afferents and respond to stimulation anywhere on the same side of the head. Instead of giving information about stimulus location, tINs sum afferent input so that a local stimulus, anywhere on the head, will recruit many tINs to fire. In response to head skin stimulation, tINs fire a brief burst of up to six spikes with the first spike occurring after 4–8 ms. When the stimulus is strong enough to initiate fictive swimming, nearly all tINs spike at least once. The tINs therefore comprise a group of skin sensory pathway interneurons responding to touch anywhere on the head and amplifying a brief, local sensory response.

Sensory pathway interneuron connections to reticulospinal neurons

If the tIN nucleus we have described does form the first link in a pathway for initiation of swimming, the next question is whether tINs excite the swimming network. During swimming, one type of interneuron plays a key role in generating the swimming rhythm and providing the excitation to drive the firing of other spinal neurons. These are descending interneurons (dINs, Li *et al.* 2006; Soffe *et al.* 2009), which form a continuous population of electrically coupled neurons (Li *et al.* 2009) extending from the spinal cord up into the hindbrain, where we consider them to be homologues of reticulospinal neurons in adults. During swimming, dINs in the hindbrain are the first neurons in the CNS to fire on each cycle (Soffe *et al.* 2009). We therefore investigated whether tINs excite dINs by making simultaneous whole-cell recordings from pairs of these neurons.

In paired recordings, tINs were identified by the characteristics described above. The dINs were recorded in

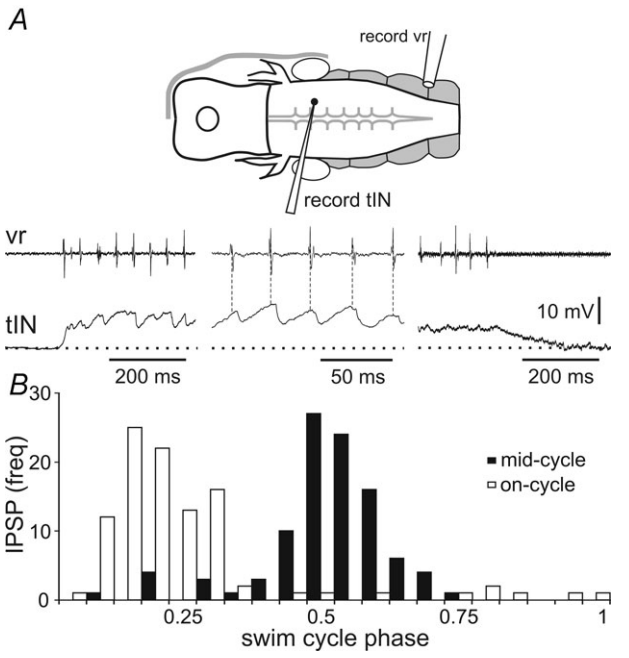

Figure 7. Activity of tINs during swimming
A, a tIN shows tonic depolarisation from the resting potential (dotted line) and receives rhythmic on-cycle IPSPs in phase with ipsilateral ventral root activity (vr) at the beginning, during, and at the end of a fictive swimming episode evoked by dimming the light. The membrane potential returns to rest about 200 ms after swimming ends. *B*, histogram showing that different tINs receive IPSPs mainly on-cycle (open bars) or mid-cycle (black bars). Data are from 10 swimming cycles for each of 20 tINs, bin size: 0.05.

the hindbrain caudal to the tINs, in rhombomeres 4–7 (see Fig. 3*A*). They were identified by their characteristically long-duration single spike response to depolarising current injections, single spike per cycle during swimming, and ventral soma with descending axon (Li *et al.* 2001, 2006, 2009). The recordings showed that in 11 of 12 pairs, a tIN action potential evoked by depolarising current injection produced a small EPSP in the dIN (Fig. 8). These EPSPs were measured for seven tIN/dIN pairs 150–350 μm apart and had latencies of 1.5 ± 0.2 ms with standard deviations ranging in individual pairs from 0.2 to 0.4 (mean 0.3), amplitudes of 2.6 ± 0.3 mV, short rise times (peak at 5.2 ± 1.1 ms) and relatively short durations (width at 50%: 14 ± 4 ms). As in some other hatchling *Xenopus* synapses (cf. Li *et al.* 2002) EPSPs were unreliable, only occurring following ~49% of tIN spikes. The EPSPs in dINs were blocked when 50 μM NBQX was added to the perfusion solution ($N = 3$ pairs; Fig. 8*C*) and are therefore glutamatergic with a significant AMPA receptor-mediated component. The short and constant latencies of these EPSPs, together with anatomy showing a close proximity of the unmyelinated tIN axons and dIN dendrites, suggest a direct, monosynaptic connection.

If individual synapses from tINs onto dINs are weak and unreliable, are they sufficient to excite dIN firing, as would be needed for head skin stimulation to initiate swimming? Our evidence shows that as the stimulus strength increases, tINs become active, and some tINs fire up to six spikes (see Fig. 2). We also know from the paired recordings that there is strong convergence of tINs onto dINs: 11/12 pairs showed synaptic connections suggesting that each dIN will be excited by most members of the tIN

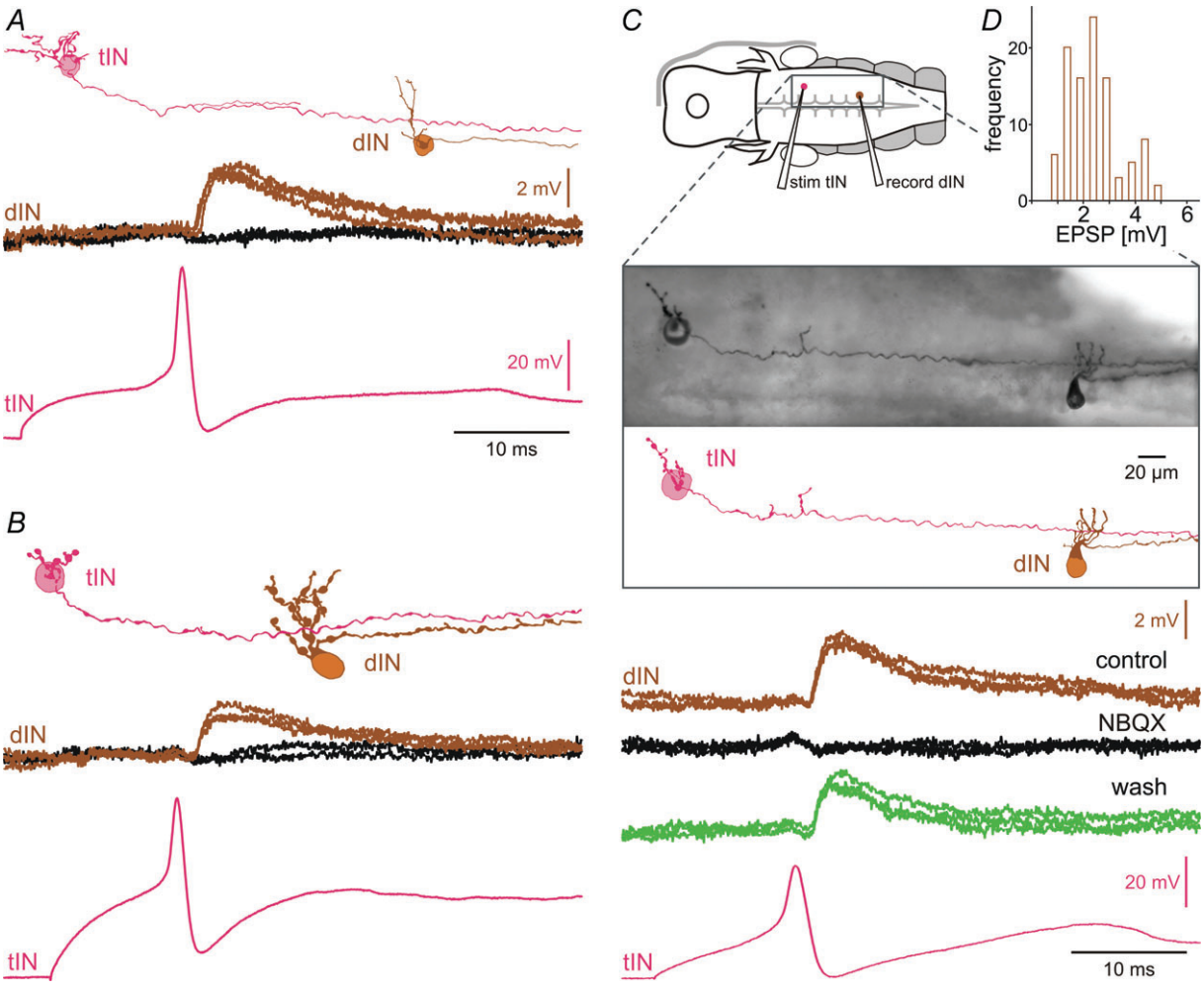

Figure 8. Synaptic connections from tINs to dINs and their pharmacology
A–C, examples of tIN/dIN paired recordings demonstrating their excitatory connection using the set-up shown in the diagram in *C*. Filled neurons viewed from the inside of the right hindbrain (rostral to the left) show tINs with descending axons and possible connections to dendrites of dINs. Current-induced spikes in tINs produce a small EPSP in dINs with a probability of about 50%. *C*, the control dIN EPSP is blocked by NBQX (50 μM) and restored after 20 min washing. Inset shows a photographic image of this pair. *D*, histogram showing the amplitudes of dIN EPSPs (data are from 10 EPSPs for each of 10 tIN/dIN pairs, bin size: 0.5 mV).

population. This means that tIN EPSPs should sum in dINs both spatially, because of this convergence of tINs onto dINs, and also temporally, because many tINs fire more than once following a stimulus. In eight paired tIN and dIN recordings, current injection into the tIN produced repetitive tIN firing and summation of tIN EPSPs in dINs. Temporal summation of these EPSPs occurred even at tIN spike frequencies less than those seen in response to head skin stimulation (Fig. 9) though it did not drive dIN firing.

Operation of the sensory pathway

To investigate whether firing in tINs is sufficient to produce firing in excitatory reticulospinal dINs, and therefore lead to swimming, we constructed a simple model of the excitatory connections between the population of tINs and individual dINs. The model was based on our measures of tIN spike times and dIN EPSP characteristics, and included stochasticity in these data.

Following a 'skin stimulus' to evoke firing in a selected population of tINs, model EPSPs summed spatially and temporally in the dIN. If the summated EPSPs following the tIN spikes depolarised the dIN membrane potential above a specified threshold potential, the dIN was deemed to fire (e.g. dotted line, Fig. 10*A*). The model was run 300 times for a range of tIN population sizes and dIN spike thresholds to estimate the probability of a dIN firing for each combination (Fig. 10*B*). Generally, the probability of dIN firing increased with increasing tIN population size and decreasing dIN spike threshold. Recently published dIN spike thresholds (Li *et al.* 2009) are distributed between –30 and –20 mV (Fig. 10*C*). This distribution of thresholds was then combined with the modelled probabilities for dIN firing at different thresholds (Fig. 10*B*) to estimate the proportion of dINs in a population that will fire, according to the size of the

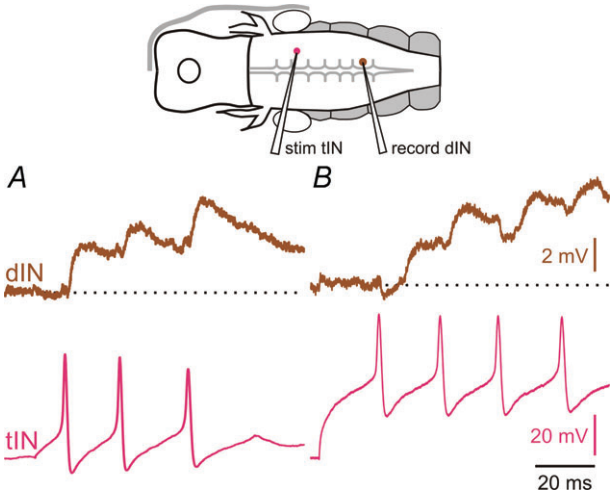

Figure 9. EPSP summation in dINs
A and *B*, tIN-evoked EPSPs in two different dINs show that they can sum temporally. Note that EPSP size can vary.

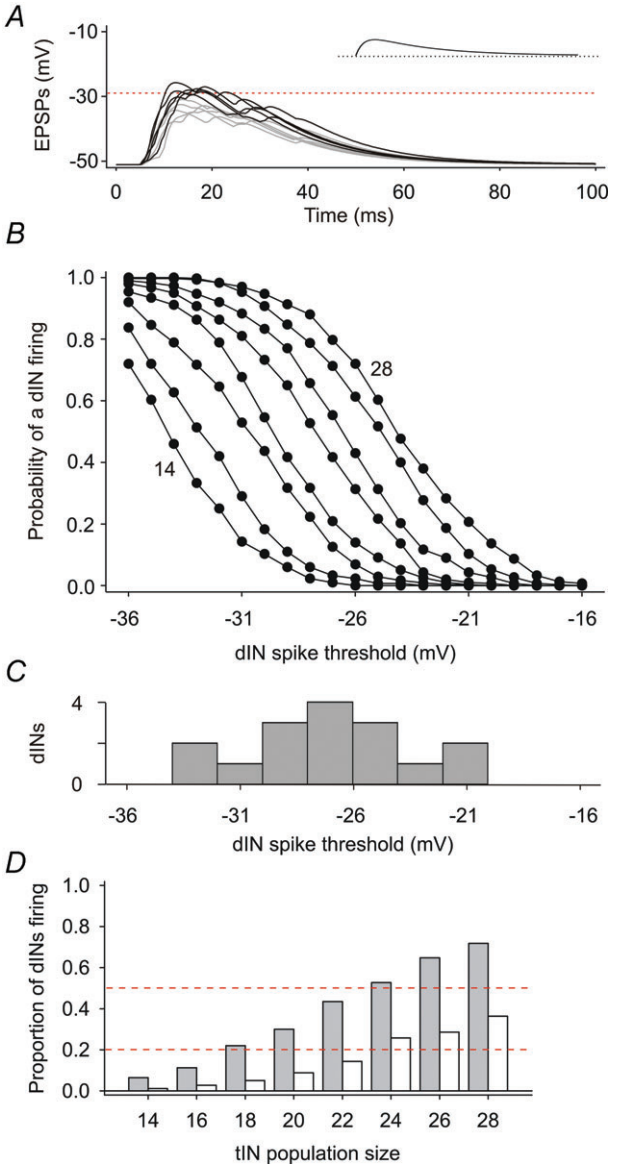

Figure 10. Modelling summation of EPSPs from the tIN population in dINs
A, ten examples of summated model EPSPs from a population of 20 tINs. Black trajectories are examples crossing a spike threshold (dotted line) set in this example at −29 mV. Grey trajectories do not cross threshold but still provide strong depolarisation. Inset shows an individual EPSP (same time scale). *B*, the probability of a dIN firing (= summated EPSP depolarising dIN above threshold) for thresholds between −16 and −36 mV; lines connect estimates for tIN populations of 14, 16, 18 . . . 28 neurons (order indicated). Each point is from 300 model runs. *C*, distribution of measured dIN spike thresholds ($N = 16$ neurons; from Li *et al.* 2009). *D*, estimated proportion of dINs firing as a result of summation of tIN EPSPs; dashed lines indicate 0.2 and 0.5 for guidance. Grey bars are based on observed tIN firing (1–5 spikes each); open bars show reduced dIN firing when tINs fire only a single spike each.

tIN population (Fig. 10*D*, grey bars). Broadly, summation of EPSPs following firing in 18–24 tINs would be expected to elicit firing in 20–50% of a dIN population (dashed lines, Fig. 10*D*). Neurobiotin backfilling estimated a tIN population size of 14–23 (see above; Fig. 1*A*). It is important to notice that summated EPSPs will depolarise individual dINs close to spike threshold even where they do not actually cross threshold and fire (e.g. Fig. 10*A*). If tINs were modelled as firing only single spikes, predicted dIN firing was much reduced (Fig. 10*D*, open bars).

As outlined above, our previous work showed that swimming is driven by the dINs, an electrically coupled population of excitatory reticulospinal neurons (Li *et al.* 2006, 2009; Soffe *et al.* 2009). Taken with this, our new evidence on the pathway to dINs following head skin stimulation suggests that swimming will occur when the dIN population becomes active. Therefore we can predict that swimming activity will be preceded by dIN firing. Recordings from 20 dINs allowed us to confirm that this is the case. All recorded dINs received EPSPs following head skin stimulation, with shortest delays of 4.4–8.8 ms (mean 6.7 ± 1.1 ms). Although some of the earliest EPSPs (<5 ms) may derive monosynaptically from sensory afferents, most of the delays were longer suggesting a disynaptic origin. We now know that a significant source of these EPSPs is the tIN population on the same side. Weaker stimuli, which did not elicit swimming, led to various patterns of EPSP summation in the dINs (grey and black traces, Fig. 11*A* and *B*). In accordance with this variable pattern of EPSP summation, firing in dINs in response to stronger stimuli also occurred with variable delays following the stimulus; the earliest spikes in each dIN occurred between 8.3 and 35.3 ms (15.0 ± 7.9 ms; Fig. 11). Stronger stimuli that led to spikes in a recorded dIN still occasionally failed to elicit swimming, indicated by the absence of a ventral root burst (blue trace, Fig. 11*B*). In these cases our interpretation is that the recorded dIN has spiked but without the whole dIN population being recruited to fire. More frequently though, stronger stimuli did elicit swimming where the first ventral root burst of swimming was preceded by dIN spikes, as were subsequent swimming motor bursts (Fig. 11*C*). In most recordings, swimming followed the first dIN spike in response to skin stimulation, though occasionally, swimming instead started after a second dIN spike (blue traces in Fig. 11*B*). Swimming only rarely began in the absence of firing in a particular, recorded dIN (3/173 episodes). We conclude that most or all of the reticulospinal dIN population fires at, or prior to, the start of swimming.

The evidence from our recordings points to a simple five stage pathway for initiating swimming activity on one side following a head skin stimulus to that side: (1) the stimulus excites trigeminal touch-sensitive afferent neurons to each fire once; (2) these sensory neurons monosynaptically excite and recruit the whole population of

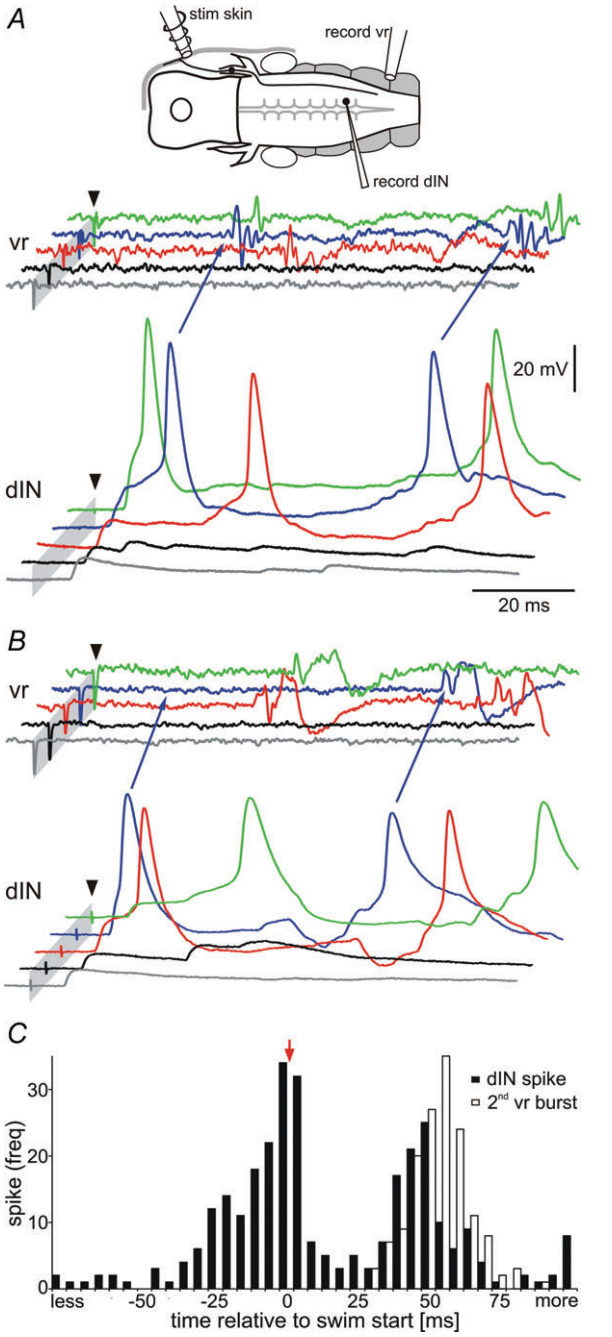

Figure 11. dINs and the start of swimming
A and *B*, two examples of dINs receiving excitation after head skin stimulation (arrowhead) at increasing strength (from bottom to top trace grey via black, red and blue to green). EPSPs in dINs sum both spatially and temporally and can lead to spike firing and the start of swimming seen in the ventral root (vr, arrows blue trace). *B*, in one case (arrows in blue trace) the first dIN spike is NOT followed by a vr burst, but the second spike is. Grey bars mark the stimulus artefacts (cropped). *C*, histogram showing dIN spike timing (black bars) relative to the first ventral root spike, which marks the start of swimming ($t = 0$; arrow). The open bars show the time to the start of the second vr burst (second cycle of swimming). dIN firing is variable but generally occurs just before ventral root activity. Data are from 150 swimming episodes from 12 dIN recordings, bin size: 5 ms.

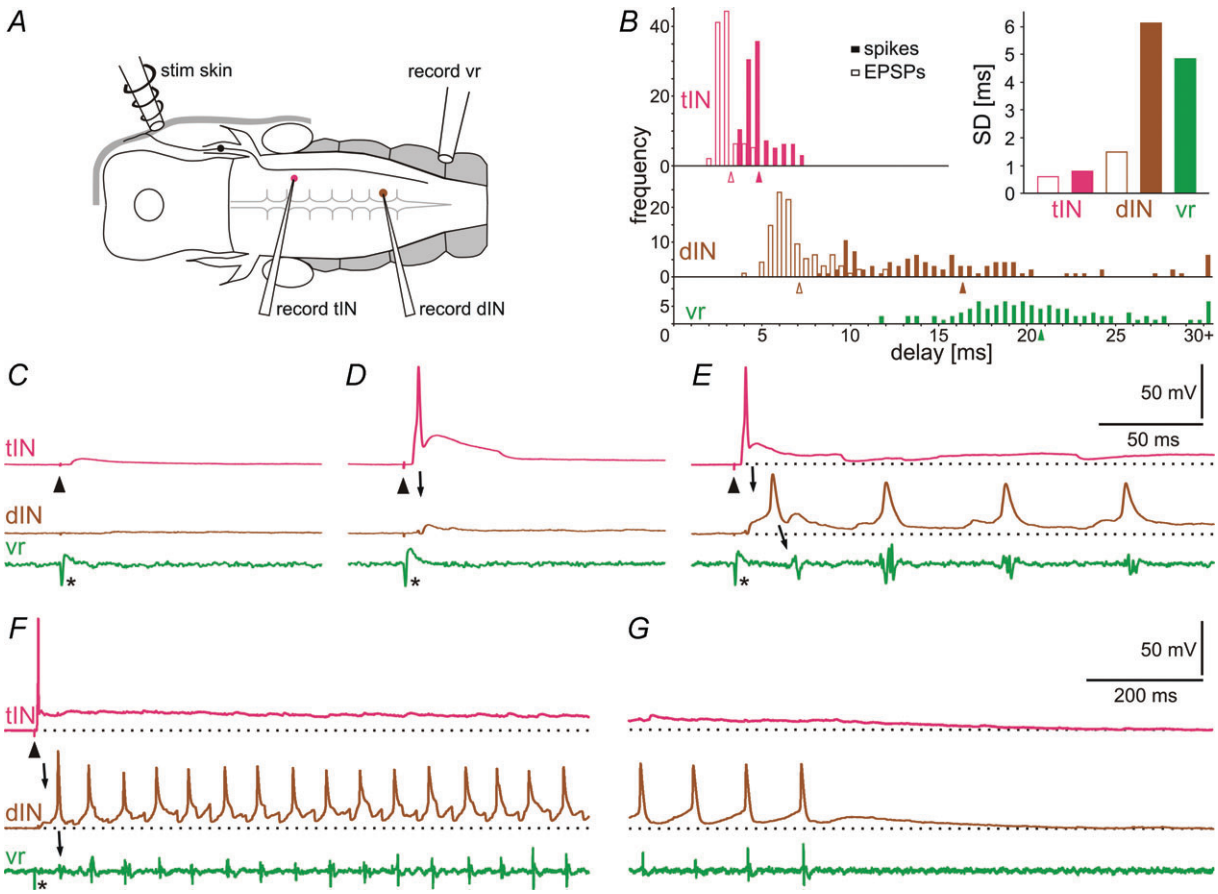

Figure 12. Initiation of swimming after head skin stimulation
A, diagram showing the position of the stimulation and recording electrodes. *B*, distribution of the response latencies from head skin stimulation to EPSPs (open bars) and spikes (filled bars) in tINs and dINs and start of swimming in vr. Note in the inset graph the much smaller standard deviations for latencies of EPSPs in tINs, spikes and EPSPs in dINs compared to the dIN spikes that are larger and similar to the onset of swimming. Data are from 10 EPSPs and spikes for each of 10 tINs, dINs and vr starts. Means are indicated by arrowheads (bin size: 0.5 ms). *C*, a weak electrical stimulus (arrowhead), insufficient to initiate swimming, leads to a short latency EPSP in the tIN. *D*, a stronger stimulus leads to a spike in the tIN followed by an EPSP in the dIN (arrow). *E*, the same strength stimulus can also lead to a spike in the tIN and dIN (arrow), followed by swimming recorded in the ventral root (vr, arrow) on the same side when the dIN fires once on each cycle. *F* and *G*, a similar response to *E* but in a different animal. Beginning (*F*) and end (*G*) of the swimming sequence shows the clear depolarisation from resting membrane potential (dotted line) of both tIN and dIN during and after fictive swimming. Asterisks mark the stimulus artefact.

about 20 tINs to each fire 1–6 times; (3) tINs in turn monosynaptically excite the electrically coupled population of reticulospinal dINs with EPSPs that sum to produce dIN firing; (4) firing of the dIN population drives the neurons active during swimming, including motoneurons; (5) motoneuron firing drives the swimming muscles.

The operation of this complete pathway from a skin stimulus via a tIN and a dIN to motor activity in a ventral root on one side of the CNS was seen in 12 paired tIN with dIN recordings (Fig. 12). The characteristics of the delays from the head skin stimulus through successive events in this pathway provide support for the steps we propose in its operation (Fig. 12*B*). Following a brief electrical stimulus to the head skin, firing in trigeminal afferents is highly synchronous (see Fig. 1*C*) and the standard deviation of the delays of EPSPs in tINs is correspondingly small, as expected if the trigeminal afferents excite them monosynaptically. The rise-time of the EPSPs in tINs is fast and invariable so the delay to the subsequent tIN spike is short, again with small standard deviations similar to those of the EPSPs. The distributions of tIN spikes and tIN EPSPs in dINs are also very much alike with the EPSPs in dINs delayed by approximately 1–2 ms, exactly as expected if this is a monosynaptic connection. There is then a much longer and more variable delay to dIN spikes which results from the considerable variation in the summation pattern

of EPSPs in dINs produced by inputs from many tINs (Fig. 11*A* and *B*). The distribution of delays to eventual motoneuron firing (ventral root (vr) activity) is similar to that of dIN spikes. Again, this might be expected since dINs have been shown to produce strong, monosynaptic excitation of motoneurons (Li *et al.* 2006).

Discussion

In this investigation of the hatchling *Xenopus* tadpole, we have used whole-cell recordings to characterise a population of hindbrain sensory pathway interneurons (tINs) which relay activity in trigeminal touch afferents to the excitatory reticulospinal neurons (dINs) that drive swimming (Li *et al.* 2006; Soffe *et al.* 2009). By doing so, we have been able to suggest how signal transfer through this sensory pathway could allow a local touch stimulus activating a few sensory neurons to be sufficient to evoke population firing in dINs, and therefore lead to swimming activity on the stimulated side. The tINs form a group of ∼20 neurons defined by their position in the 2nd to 4th rhombomeres caudal to the entry of the trigeminal nerve on each side of the hindbrain, by their unipolar somata with dendrites, and by a long, ipsilateral, descending axon of relatively large diameter. We have shown that individual tINs are excited to fire by trigeminal afferents in response to brief electrical stimuli, mimicking touch, anywhere on the same side of the head. In turn, paired whole-cell recordings show that tINs excite ipsilateral reticulospinal dINs via their descending axons. Both these synapses are monosynaptic and glutamatergic. Several lines of evidence identify the tINs as a major, ipsilateral trigeminal-to-reticulospinal relay nucleus for touch stimuli: the discrete nature of the tIN population revealed by backfilling; the consistent properties of these neurons; their monosynaptic connections from head skin afferents and onto the reticulospinal dINs. Previous whole-cell recordings have shown that dINs make strong, direct excitatory connections to spinal motoneurons and CPG interneurons (Li *et al.* 2006), so a complete sensory to motor pathway has now been defined (Fig. 13).

Trigeminal touch pathway

How are signals transformed as they pass through the trigeminal touch pathway? The head skin afferents have small receptive fields (0.015 mm^2) with little overlap (Hayes & Roberts, 1983), and we have shown that local electrical stimulation will only excite one or a small number of trigeminal sensory neurons. In contrast, the tIN sensory relay interneurons fire in response to stimuli anywhere on the head. Several lines of evidence are presented here about the convergence of head skin afferents onto tINs: extracellular unit recordings and intracellular recordings from single tINs both show responses to stimuli (mechanical and electrical, respectively) at separate locations anywhere on the same side of the head; simultaneous recordings from pairs of tINs show coincident appearance of afferent EPSPs to the same stimuli; and recordings in individual animals show responses in multiple tINs to skin stimuli given at a single site. Our conclusion from this evidence is that each touch afferent contacts most or perhaps all the tINs on the same side of the head and, correspondingly, each tIN is strongly excited by most or all of the touch afferents innervating the same side. This pattern of connection, taken together with the high probability of tINs firing in response to a stimulus, provides a considerable signal convergence and results in amplification of the sensory signal because spikes in a few afferents produce spikes in many tINs. A similar amplification was previously suggested for signals from trunk and tail skin afferents, where individual touch sensory Rohon-Beard neurons excite firing in a population of sensory pathway 'dorsolateral interneurons' some of which mediate a flexion reflex (Clarke & Roberts, 1984; Li *et al.* 2003, 2004). However, there is a significant difference. Dorsolateral interneuron firing is terminated after a single spike by short latency inhibition so the amplification simply reflects the greater number of sensory interneurons firing. On the other hand, our evidence indicates that tINs further amplify activity in trigeminal afferents through each firing up to six times, extending the effective duration of sensory discharge and potential for subsequent summation (Fig. 2).

We are proposing that firing of the tIN population in response to touch will then produce firing in the excitatory

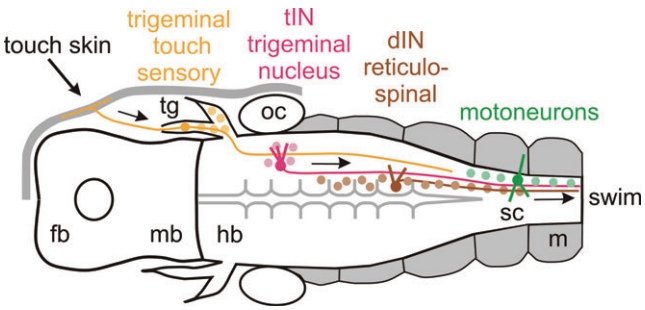

Figure 13. Proposed step-by-step trigeminal pathway initiating locomotion
Dorsal view diagram of the tadpole head showing the elements of the trigeminal swim-initiating pathway (arrows): (1) local stimulation of the head skin excites a few touch-sensitive trigeminal sensory neurons (<5); (2) these directly excite and recruit the whole tIN population (∼20); (3) tINs directly excite the reticulospinal hindbrain dINs which are electrically coupled so firing in a few recruits the whole dIN population (∼160); (4) dIN firing initiates rhythm generation and drives all the spinal neurons active during swimming, including motoneurons (∼270); (5) motoneuron firing (vr) drives the swimming muscles. fb, forebrain; hb, hindbrain; mb, midbrain; m, muscles; oc, otic capsule; sc, spinal cord; tg, trigeminal ganglion.

reticulospinal dINs, leading to swimming. However, the EPSPs produced in dINs by single tIN spikes are very small and only ∼50% reliable. If most tINs fire following a stimulus and some of them fire multiple spikes, then tIN excitation of dINs will sum both spatially and temporally. Such patterns of summation are unpredictable and hard to investigate quantitatively. We therefore used a simple synapse model to ask whether firing in a tIN population would be sufficient to excite individual dINs above spike threshold and make them fire. The model showed that a population of ∼20 tINs could produce firing in ∼25% of the dINs and that dINs that did not fire would be depolarised close to threshold. Since neurons in the hindbrain dIN population are electrically coupled (Li *et al.* 2009) and make mutual excitatory chemical synapses (Li *et al.* 2006), it is plausible that tIN excitation following local head skin stimulation is indeed sufficient to recruit firing in the whole dIN population. We suggested that this is of key importance because dIN firing is the necessary step for initiating swimming, and our evidence supports this. It had already been shown that, on either side of the CNS, dINs are active first on each cycle during swimming (Soffe *et al.* 2009). We have now also shown that firing in the dIN population precedes motoneuron activity at the start of each episode of swimming. Since dINs do not receive significant direct input from primary afferents, we suggest that the tIN to dIN pathway we describe plays a key role in the initiation of swimming by trigeminal afferents.

Initiation of locomotion

Trigeminal stimulation can initiate locomotion in other vertebrates including mammals. The widely accepted view is that activity in descending reticulospinal pathways is needed to drive spinal locomotor patterns (Orlovsky *et al.* 1999; Goulding, 2009). In the lamprey, candidate relay neurons have been described with somata lying in the large, descending trigeminal tract and projecting to reticulospinal nuclei (Viana Di Prisco *et al.* 2005). Some lie at around the level of the VIIIth cranial nerve, like the tINs, but others are more caudal. The connections and physiological characteristics of these neurons have not yet been investigated. Unlike the tadpole, where tIN projections are exclusively ipsilateral, there are both ipsilateral and contralateral projections among the candidate relay neurons in the lamprey. In the cat, Noga and co-workers (Noga *et al.* 1988, 1991) suggested that trigeminal stimulation activates neurons in the medial reticular formation, and therefore spinal cord locomotor circuitry, via the pontomedullary locomotor region, a region closely associated with the trigeminal spinal nucleus (in turn associated with nociceptive stimuli). However, only in the tadpole has a pathway from trigeminal afferents to reticulospinal neurons been fully characterised.

Two features of the tINs have further significance for swim initiation. The first is that their projections are exclusively ipsilateral. Unlike the axons of the trigeminal descending spinal tract in adult frogs which cross in the first two spinal segments (Matesz & Székely, 1978), the axons of tadpole trigeminal afferents do not cross (Hayes & Roberts, 1983). For a unilateral stimulus to elicit swimming bilaterally, this means that the trigeminal afferents and/or tINs must excite neurons in the hindbrain with crossing axons which in turn excite contralateral dINs. This part of the swim initiation pathway remains to be identified. However, in the tadpole and the lamprey, swimming-like motor activity can be generated by a single side of the nervous system (Kahn & Roberts, 1982; Soffe, 1989; Cangiano & Grillner, 2003). We have recently investigated the roles for NMDA-dependent cellular rhythmicity in the population of reticulospinal dINs in single-sided 'swimming' (Li *et al.* 2010). Our evidence suggests that the head skin tIN pathway to dINs could initiate such single-sided swimming. The second feature is that descending tIN axons extend a significant distance into the spinal cord, where we presume they make synapses. Perhaps these serve to 'prime' spinal cord neurons before the descending reticulospinal (dIN) excitation arrives at the start of swimming. Direct descending effects of trigeminal stimuli on the spinal cord locomotor system have also been suggested in the cat (Noga *et al.* 1988, 1991) and rat (Vinay *et al.* 1995).

In addition to their amplifier role, the tINs provide a step in the pathway where inhibition can act and modulate the signal transfer, as is common across the animal kingdom in sensory systems controlling locomotion (see: Poulet & Hedwig, 2007; Crapse & Sommer, 2008). Short latency inhibition may thus limit firing to strong stimuli and inhibition during swimming may gate out inappropriate responses.

The precise neuronal pathways initiating locomotion have only previously been defined in two invertebrates. In the leech, a neuron-by-neuron pathway for swim initiation by mechanical stimuli has identified two 'trigger' and many 'gating' neurons (Brodfuehrer & Friesen, 1986). In the marine mollusc *Tritonia*, a neuronal pathway initiating swimming has also been defined in response to contact by a starfish (Frost *et al.* 2001). In both cases, sensory neurons excite central nervous trigger neurons (active before locomotion starts), which then activate gating neurons (active during locomotion) to convert a brief stimulus into prolonged firing that drives the rhythm-generating circuits of the locomotor system (see Stein, 1978). Surprisingly, the pathway in the tadpole (Fig. 13), a simple vertebrate, may be more direct if excitation from tINs triggers the firing of reticulospinal dINs, which then act both as gating neurons and oscillator neurons driving the swimming rhythm (Li *et al.* 2006, 2010; Soffe *et al.* 2009).

Conclusion

The tIN population appears to constitute an important, early, sensory trigeminal nucleus of unimodal neurons. All respond strongly to ipsilateral head skin stimuli but not to stimuli from the opposite side of the head or from trunk and tail skin, and show negligible response to light dimming, a stimulus detected by the pineal eye and which can also initiate swimming (Roberts, 1978). Lastly, tINs show no response to skin impulses, conducted epithelial impulses generated by noxious stimuli whose signals are known to enter the CNS via the trigeminal nerve and to be able to initiate swimming (Roberts, 1969, 1996). The tINs do not therefore constitute a wider integration centre for sensory initiation of swimming but instead parallel the sensory interneurons of the spinal cord, in particular the ipsilaterally projecting dorsolateral ascending interneurons which specifically relay trunk skin touch information (Li *et al.* 2004). Presumably, the primitive trigeminal sensory nucleus formed by the tINs is part of the incompletely known descending trigeminal nucleus of adult anurans (ten Donkelaar *et al.* 1981), but its relationship to mammalian nuclei is currently obscure.

Our results characterise hindbrain trigeminal interneurons in a simple disynaptic pathway by which trigeminal touch afferents excite the reticulospinal neurons that drive locomotion. This pathway may therefore form the ipsilateral part of a simple, ancestral route for the initiation of swimming. If so, then equivalent elements may still exist in higher vertebrates, including mammals, underlying more complex initiation pathways.

References

Aoki M & Mori S (1981). Locomotion elicited by pinna stimulation in the acute precollicular post-mammillary decerebrate cat. *Brain Res* **214**, 424–428.

Beresovskii VK & Bayev KV (1991). Locomotor regions of the brain stem: a new hypothesis of locomotion initiation. In *Locomotor Neural Mechanisms in Arthropods and Vertebrates*, ed. Armstrong DM & Bush BMH, pp. 260–268. Manchester University Press, Manchester and New York.

Boothby KM & Roberts A (1995). Effects of site of tactile stimulation on the escape swimming responses of hatchling *Xenopus laevis* embryos. *J Zool* **235**, 113–125.

Brodfuehrer PD & Friesen WO (1986). From stimulation to undulation: A neuronal pathway for the control of swimming in the leech. *Science* **234**, 1002–1004.

Cangiano L & Grillner S (2003). Fast and slow locomotor burst generation in the hemispinal cord of the lamprey. *J Neurophysiol* **89**, 2931–2942.

Clarke JDW & Roberts A (1984). Interneurones in the *Xenopus* embryo spinal cord: sensory excitation and activity during swimming. *J Physiol* **354**, 345–362.

Crapse TB & Sommer MA (2008). Corollary discharge across the animal kingdom. *Nat Rev Neurosci* **9**, 587–600.

Dubuc R, Brocard F, Antri M, Fenelon K, Gariepy JF, Smetana R, Menard A, Le Ray D, Viana Di Prisco G, Pearlstein E, Sirota MG, Derjean D, St-Pierre M, Zielinski B, Auclair F & Veilleux D (2008). Initiation of locomotion in lampreys. *Brain Res Rev* **57**, 172–182.

Edwards DH, Heitler WJ & Krasne FB (1999). Fifty years of a command neuron: The neurobiology of escape behavior in the crayfish. *Trends Neurosci* **22**, 153–161.

Foster RG & Roberts A (1982). The pineal eye in *Xenopus laevis* embryos and larvae – A photoreceptor with a direct excitatory effect on behavior. *J Comp Physiol A* **145**, 413–419.

Frost WN, Hoppe TA, Wang J & Tian L-M (2001). Swim initiation neurons in *Tritonia diomedea*. *Am Zool* **41**, 952–961.

Goulding M (2009). Circuits controlling vertebrate locomotion: moving in a new direction. *Nat Rev Neurosci* **10**, 507–518.

Grillner S, Wallen P, Saitoh K, Kozlov A & Robertson B (2008). Neural bases of goal-directed locomotion in vertebrates – An overview. *Brain Res Rev* **57**, 2–12.

Hayes BP & Roberts A (1983). The anatomy of two functional types of mechanoreceptive 'free' nerve-ending in the head skin of *Xenopus* embryos. *Proc R Soc Lond Biol Sci* **218**, 61–76.

Jordan LM, Liu J, Hedlund PB, Akay T & Pearson KG (2008). Descending command systems for the initiation of locomotion in mammals. *Brain Res Rev* **57**, 183–191.

Kahn JA & Roberts A (1982). The central nervous origin of the swimming motor pattern in embryos of *Xenopus laevis*. *J Exp Biol* **99**, 185–196.

Korn H & Faber DS (2005). The Mauthner cell half a century later: A neurobiological model for decision-making? *Neuron* **47**, 13–28.

Kyriakatos A, Mahmood R, Ausborn J, Porres CP, Büschges A & El Manira A (2011). Initiation of locomotion in adult zebrafish. *J Neurosci* **31**, 8422–8431.

Li W-C, Perrins R, Soffe SR, Yoshida M, Walford A & Roberts A (2001). Defining classes of spinal interneuron and their axonal projections in hatchling *Xenopus laevis* tadpoles. *J Comp Neurol* **441**, 248–265.

Li W-C, Roberts A & Soffe SR (2009). Locomotor rhythm maintenance: electrical coupling among premotor excitatory interneurons in the brainstem and spinal cord of young *Xenopus* tadpoles. *J Physiol* **587**, 1677–1693.

Li W-C, Roberts A & Soffe SR (2010). Specific brainstem neurons switch each other into pacemaker mode to drive movement by activating NMDA receptors. *J Neurosci* **30**, 16609–16620.

Li W-C, Soffe SR & Roberts A (2002). Spinal inhibitory neurons that modulate cutaneous sensory pathways during locomotion in a simple vertebrate. *J Neurosci* **22**, 10924–10934.

Li W-C, Soffe SR & Roberts A (2003). The spinal interneurons and properties of glutamatergic synapses in a primitive vertebrate cutaneous flexion reflex. *J Neurosci* **23**, 9068–9077.

Li W-C, Soffe SR & Roberts A (2004). Dorsal spinal interneurons forming a primitive, cutaneous sensory pathway. *J Neurophysiol* **92**, 895–904.

Li W-C, Soffe SR, Wolf E & Roberts A (2006). Persistent responses to brief stimuli: Feedback excitation among brainstem neurons. *J Neurosci* **26**, 4026–4035.

Matesz C & Székely G (1978). The motor column and sensory projections of the branchial cranial nerves in the frog. *J Comp Neurol* **178**, 157–175.

Nieuwkoop PD & Faber J (1956). *Normal Tables of Xenopus laevis (Daudin)*. North Holland, Amsterdam.

Noga BR, Kettler J & Jordan LM (1988). Locomotion produced in mesencephalic cats by injections of putative transmitter substances and antagonists into the medial reticular-formation and the pontomedullary locomotor strip. *J Neurosci* **8**, 2074–2086.

Noga BR, Kriellaars DJ & Jordan LM (1991). The effect of selective brain-stem or spinal-cord lesions on treadmill locomotion evoked by stimulation of the mesencephalic or pontomedullary locomotor regions. *J Neurosci* **11**, 1691–1700.

Orlovsky GN (1970). Work of reticulo-spinal neurones during locomotion. *Biophysics* **15**, 761–771.

Orlovsky GN, Deliagina TG & Grillner S (1999). *Neuronal Control of Locomotion: From Mollusc to Man*. Oxford University Press, Oxford.

Poulet JFA & Hedwig B (2007). New insights into corollary discharges mediated by identified neural pathways. *Trends Neurosci* **30**, 14–21.

Roberts A (1969). Conducted impulses in skin of young tadpoles. *Nature* **222**, 1265–1266.

Roberts A (1978). Pineal eye and behaviour in *Xenopus* tadpoles. *Nature* **273**, 774–775.

Roberts A (1980). The function and role of two types of mechanoreceptive 'free' nerve endings in the head skin of amphibian embryos. *J Comp Physiol A* **135**, 341–348.

Roberts A (1990). How does a nervous system produce behaviour? A case study in neurobiology. *Sci Prog* **74**, 31–51.

Roberts A (1996). Trigeminal pathway for the skin impulse to initiate swimming in hatchling *Xenopus* embryos. *J Physiol* **493.*P***, P40–P41.

Safronov BV, Pinto V & Derkach VA (2007). High-resolution single-cell imaging for functional studies in the whole brain and spinal cord and thick tissue blocks using light-emitting diode illumination. *J Neurosci Methods* **164**, 292–298.

Soffe SR (1989). Roles of glycinergic inhibition and N-methyl-D-aspartate receptor mediated excitation in the locomotor rhythmicity of one half of the *Xenopus* embryo central nervous system. *Eur J Neurosci* **1**, 561–571.

Soffe SR, Roberts A & Li WC (2009). Defining the excitatory neurons that drive the locomotor rhythm in a simple vertebrate: insights into the origin of reticulospinal control. *J Physiol* **587**, 4829–4844.

Stein PSG (1978). Motor systems, with specific reference to the control of locomotion. *Ann Rev Neurosci* **1**, 61–81.

Stephenson-Jones M, Samuelsson E, Ericsson J, Robertson B & Grillner S (2011). Evolutionary conservation of the basal ganglia as a common vertebrate mechanism for action selection. *Curr Biol* **21**, 1081–1091.

ten Donkelaar HJ, de Boer-van Huizen R, Schouten FTM & Eggen SJH (1981). Cells of origin of descending pathways to the spinal cord in the clawed toad (*Xenopus laevis*). *Neuroscience* **6**, 2297–2312.

Viana Di Prisco G, Boutin T, Petropoulos D, Brocard F & Dubuc R (2005). The trigeminal sensory relay to reticulospinal neurones in lampreys. *Neuroscience* **131**, 535–546.

Vinay L, Cazalets JR & Clarac F (1995). Evidence for the existence of a functional polysynaptic pathway from trigeminal afferents to lumbar motoneurons in the neonatal rat. *Eur J Neurosci* **7**, 143–151.

Author contributions

The experiments were performed in the neurobiology lab at the University of Bristol by E.B. and A.R. The model was constructed by S.R.S. All three authors contributed to the conception and design of experiments, analysis of data and writing the manuscript. All authors approved the final version of the manuscript.

Acknowledgements

We thank Drs Wen-Chang Li and James Poulet for helpful comments on the manuscript. This work was supported by the BBSRC (grant BB/G006652/1).